Insights into self-healing behavior and mechanism of dicalcium phosphate dihydrate coating on biomedical Mg

Qiangsheng Dong[a,b], Xingxing Zhou[a], Yuanjia Feng[a], Kun Qian[a,b], Huan Liu[c], Mengmeng Lu[d], Chenglin Chu[a,b], Feng Xue[a,b,*], Jing Bai[a,b,**]

[a] School of Materials Science and Engineering, Jiangsu Key Laboratory for Advanced Metallic Materials, Southeast University, Nanjing, 211189, China
[b] Institute of Medical Devices (Suzhou), Southeast University, Suzhou, 215000, China
[c] College of Mechanics and Materials, Hohai University, Nanjing, 211100, China
[d] Department of Oral Implantology, Affiliated Hospital of Stomatology, Nanjing Medical University, Nanjing, 210029, China

ABSTRACT

Self-healing coatings have been developed as smart surface coatings for Mg and its alloys to retain local corrosion from the coating damages. In this study, we prepared dicalcium phosphate dihydrate (DCPD) coating on biomedical Mg, and found that the artificial scratches in DCPD coating can be efficiently sealed by anti-corrosive products in both Hank's and normal saline (NS) solutions. Besides, the in-depth study revealed that DCPD was served as not only a physical barrier but also a self-healing agent, demonstrating an autonomous self-healing coating without embedded extra corrosion inhibitors. Moreover, Hank's solution provided foreign-aid film-forming ions to promote self-healing behavior. The findings might offer new opportunities for further studies and applications of efficient self-healing coatings on biodegradable Mg implants.

1. Introduction

Magnesium (Mg) and its alloys have been considered as a new generation of biodegradable metals [1–3]. Their many excellent performances, such as favorable biocompatibility, great biodegradability, favorable bone conductivity, and appropriate mechanical properties, have attracted much attention from researchers and clinicians [3–5]. However, the uncontrollable corrosion of Mg alloys is still a serious issue limiting their clinical applications [6]. To avoid this weakness, various surface protective coatings have been developed for clinical requirements [7–10].

Surface modifications have advantages in the control of the undesired corrosion rate of Mg-based biomaterials. However, surface scratches on implants seem unavoidable during surgery, and the partial damages provide pathways for the intake of the aggressive solution and lead to severe local corrosion and even premature coating failures [11,12]. Self-healing coatings were defined as a kind of smart coatings that can repair the coating defects and recover the coating properties on the basis of initiative or passivity [13]. Recently, various new self-healing coatings have been designed on Mg and its alloys [14–22], equipped with both anti-corrosive property and self-healing functionality. The self-healing coatings are often designed by embedding self-healing agents or corrosion inhibitors in the anti-corrosive coatings [13]. But more self-healing coatings for industrial applications have chosen some toxic self-healing agents or corrosion inhibitors, including cerium ions [16], benzotriazole [17], 8-hydroxyquinoline [18] and so on, which can hardly be applied for biomedical applications. Compared with these coatings, biomedical self-healing coatings have emerged later, which put forward a high demand for good biological properties. There has been some significant progress made in coating designs. For instance, Zhao et al. [20] fabricated self-healing multilayer film based on SiO$_2$ and CeO$_2$ nanoparticles, but the biocompatibility was unclear because of CeO$_2$ in the film. Furthermore, Xiong et al. [21,22] established biomedical self-healing coatings with silk fibroin combined with K$_3$PO$_4$ or phytic acid. These coatings exhibited not only good biocompatibility but also self-healing functionality by embedding extra corrosion inhibitions in coatings [13,21]. No doubt, these recent works have greatly promoted the development of biomedical Mg. However,

---

the research progress is still in the early stage, and it is worth providing theoretical and experimental supports for self-healing coatings in further clinical applications.

The development of biomedical self-healing coatings should take the bioactivity into first consideration. In the bioactive calcium phosphate coating system, hydroxyapatite (HA) and octacalcium phosphate (OCP) coatings have been reported to have self-healing ability on Mg and its alloys [12]. Self-healing function is discovered on these common biomedical coatings, and there are no doubts that this study is more beneficial to promote clinical applications of biomedical self-healing coatings. Besides, dicalcium phosphate dihydrate (DCPD) coating is also a representative calcium phosphate coating, which has been reported to display outstanding biocompatibility as an intermediate in bone mineralization [23]. Compared with HA and OCP, DCPD exhibits many noteworthy special features, as follows: (1) Chemical property. DCPD has larger solubility and higher supplement for Ca^{2+} and PO_4^{3-} ions available near the implant [24,25]; (2) Facile preparation. DCPD is easy to coat on Mg-based implants even with intricate shapes at room/medium temperature [26,27]. Herein, the chemical property can endow DCPD with self-healing ability derived from a higher supplement for Ca^{2+} and PO_4^{3-} ions; facile preparation will be helpful to further clinical applications. Recently, there are no reports on the self-healing ability of DCPD coatings, but the self-healing functionality is worthy of study to further widen the clinical application fields.

Therefore, DCPD coating was facilely prepared on pure Mg in this work, and exhibited not only good corrosion protection but also self-healing capability in both Hank's and normal saline (NS) solutions. It was demonstrated that DCPD was acted as not only a physical barrier but also a self-healing agent, indicating an autonomous self-healing coating without embedded extra corrosion inhibitions. These research findings might explore the self-healing capability of DCPD coatings on biomedical Mg, and open new opportunities to develop novel coatings with autonomous self-healing for a stable service of biomedical Mg implants in clinical applications.

2. Materials and methods

2.1. Coating preparation

The raw materials were as-cast pure Mg plates (99.95 wt%, Fe < 0.003 wt%) with a dimension of 15 mm × 25 mm × 5 mm. The plate surfaces were ground up to 2000 grit SiC sandpapers. Then Mg plates were immersed in 1 mol L^{-1} NaOH solution at 60 °C for 30 min to clean surface, and then Mg plates were acid-cleaned in 10 vol% hydrofluoric acid solution for surface removal and activation, then washed with deionized water, and dried in cold air. Subsequently, the coating formation was carried out in Ca–P electrolyte (0.1 mol L^{-1} Ca$(NO_3)_2$·4H$_2$O and 0.06 mol L^{-1} NH$_4$H$_2$PO$_4$, pH = 3.55 ± 0.10) at 25 °C. The pretreated samples were dipped in the Ca–P electrolyte for 60 min to obtain Ca–P coatings prepared on pure Mg plates. Fig. 1 illustrates the facile preparation process of Ca–P coatings on Mg plates.
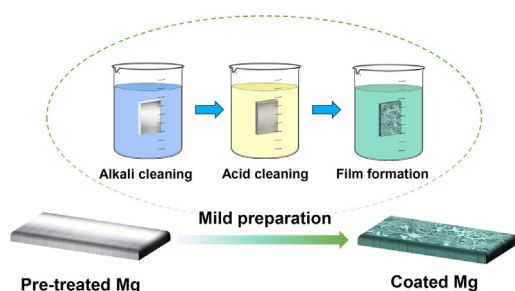

Fig. 1. Schematic diagram of the facile preparation process of Ca–P coatings.

2.2. Surface characterizations

The surface and cross-section morphologies were observed by a field emission scanning electron microscope (SEM, FEI Sirion 200), and the corresponding elementary composition was detected by the equipped energy-dispersive X-ray spectroscopy (EDS, Oxford Azter X-Max 80). The phase structure was identified by an X-ray diffractometer (XRD, Bruker D8-Discover) at a scanning rate of 8°/min as well as a transmission electron microscope (TEM, Tecnai G2 20). Besides, the surface functional groups were identified via an attenuated total internal reflectance Fourier transform infrared spectrometer (FTIR, Thermo Scientific Nicolet iS10).

2.3. Degradation behavior

The degradation behavior was evaluated by both electrochemical methods and in-vitro immersion tests in Hank's and NS solutions at 37 ± 0.5 °C. The Hank's solution was composed of NaCl (8.0 g L^{-1}), KCl (0.4 g L^{-1}), NaHCO$_3$ (0.35 g L^{-1}), MgCl$_2$·6H$_2$O (0.1 g L^{-1}) MgSO$_4$·7H$_2$O (0.06 g L^{-1}), CaCl$_2$ (0.14 g L^{-1}), Na$_2$HPO$_4$ (0.06 g L^{-1}), KH$_2$PO$_4$ (0.06 g L^{-1}) and glucose (1 g L^{-1}) [28], while NS solution consisted of NaCl (9 g L^{-1}) [29]. Prior to the evolution of the anti-corrosive property, the pH values of Hank's and NS solution were adjusted to 7.4 by the addition of HCl or NaOH solution.

Electrochemical corrosion methods were performed on an Ametek PARSTAT 3000A-DX electrochemical workstation, and a three-electrode cell was applied including the specimen with an exposed area of 1 cm^2 as a working electrode, a saturated calomel electrode (SCE) as a reference electrode, and a platinum plate as an auxiliary electrode. Prior to electrochemical impedance spectroscopy (EIS) and potentiodynamic polarization (PDP) measurements, the electrodes were immersed in physiological solutions for 20 min to stabilize open circuit potential (E_{ocp}). To ensure data validity [30], PDP curves were separated into anodic and cathodic branches at a constant scanning rate of 1 mV s^{-1}, in which cathodic PDP was scanned from +0.02 V vs E_{ocp} to −2.00 V vs SCE, and anodic PDP was scanned from −0.02 V vs E_{ocp} to −1.00 V vs SCE. The method could avoid a shift in corrosion potential (E_{corr}) resulting from great mass transfer near to the electrodes when the applied potential is scanned from cathodic polarization to anodic polarization [30]. Besides, EIS plots with ten points per decade were collected in the scanning frequency range from 100 kHz to 100 mHz with 10 mV ac amplitude vs E_{ocp}. The collected EIS plots were fitted and analyzed by Zsimpwin software. Moreover, the coated samples were immersed in Hank's and NS solution at 37 ± 0.5 °C, and the evolved hydrogen gas was collected by an inverted buret during immersion. Furthermore, the microstructure evolutions were characterized by XRD, FTIR, TEM, SEM and EDS to reveal self-healing mechanism.

2.4. Evaluation of self-healing capacity

Prior to the evaluation of self-healing capacity, the coating surface was scratched to an I-shaped mark by a knife applied with a constant load. The ratio of the scratch length to the coating surface area was set as 1 cm: 5 cm^2, and the scratch width was 50 μm. The surface and cross-section morphologies of scratched coatings are provided in Fig. S1 of **Supplementary Material**.

Scanning vibrating electrode technique (SVET) measurements were performed in a scanning electrochemical workstation (Ametek VersaSCAN, USA) to reveal the evolution of local corrosion behaviors in scratches. A Pt–Ir electrode probe (10 μm) was placed on the assigned surface at a distance of about 100 μm. The 3D mappings of ionic fluxes in a square array of 21 × 21 points were collected above the exposed area (2 × 2 mm^2) containing the scratches. The scratched DCPD coated samples were monitored during the immersion for 4 h. The current density was calculated as Equation (1) [31].

$$i = -k\frac{\Delta V}{\Delta r} \qquad (1)$$

Where i is current density, k is the solution conductivity (k was measured using SX650 conductivity meter; 17.5 ± 0.2 ms cm^{-1} in Hank's solution; 16.5 ± 0.2 ms cm^{-1} in NS solution), ΔV is the measured reaction potential difference in amplitude of Δr (set as 30 μm in the experiment).

Then the scratched samples were immersed in Hank's and NS solutions, and the hydrogen evolution and EIS results were collected during immersion. To investigate the relevant self-healing mechanism, surface and cross-section morphologies as well as the related elemental analysis were detected by SEM equipped with EDS.

2.5. pH stimulus-responsive behavior

The pH-sensitive behavior was evaluated by thermodynamic analysis and ion release experiments. The thermodynamic parameters were calculated using PHREEQC software [32] to reveal the association/dissociation reactions of Ca–P compounds in physiological solutions. The details on thermodynamic calculation methods were provided in **Supplementary Material**. Furthermore, to investigate Ca and P element release from DCPD in different pH conditions, the DCPD-coated samples were immersed in deionized water for 1,3,5 and 7 days, in which the pH of deionized water was adjusted to 7.4, 8.0, 9.0 and 10.0 by the addition of NaOH solution (0.01 mol/L). The solutions were analyzed by inductively coupled plasma mass spectrometry (ICP-OES, Thermo Scientific iCP 6500).

3. Results

3.1. Coating characterizations

Fig. 2 displays the DCPD coating characterizations. The predominance area diagram for coating formation was calculated using the MEDUSA software package [33], as shown in Fig. 2(a). When immersed in the acidic saturated Ca–P electrolyte (pH = 3.55 ± 0.10), the metallic Mg is dissolved along with local alkalinity around Mg surface

[34]. Then, CaHPO$_4$·2H$_2$O (DCPD) coating tends to be preferentially formed on Mg plates. The surface and cross-section morphologies of Ca–P coating are demonstrated in Fig. 2(b–d), reflecting that the coating is formed as vertical and tilted micro-sheets on pure Mg plates. The coating is approximately 30 μm thick, which can provide corrosion protection for Mg plates. The bonding strength between coating and substrate is approximately 5.2 MPa, as shown in Fig. S2. Besides, the micro-scale structure contributes to super hydrophilicity (Movie S1), providing a compatible platform for cell adhesion and cell proliferation [35]. The EDS results, corresponding to the selected regions in SEM, are summarized in Fig. S3. Herein, the EDS results in Region (A, B) exhibit that the Ca–P coating is mainly composed of O, Ca, and P elements, in which Ca/P atomic ratio is approximately equal to 1 (in Fig. S3). To identify the phase structure, Ca–P coated Mg plate was characterized by XRD. In Fig. 2(e), where the peaks of DCPD (Brushite, CaHPO$_4$·2H$_2$O, JCPDS No.11–0293) and Mg (JCPDS No.35–0821) can be indexed. Besides, FTIR results of as-fabricated coating in Fig. 2(f) shows OH in H$_2$O and HPO$_4^{2-}$ groups [36–38]. Absorption bands at 3151-3531 cm^{-1} are attributed to two O–H stretching doublets. H$_2$O bending bands are located at 1674 cm^{-1} while libration bands correspond to the peaks at 780 cm^{-1} and 649 cm^{-1}. Besides, the phosphate triplet is confirmed according to the peaks at 1119 cm^{-1}, 1053 cm^{-1} and 983 cm^{-1}. Adsorptions at 1203 cm^{-1} and 869 cm^{-1} are related to P–OH in-plane bending and stretching modes, respectively. All the above results demonstrate that DCPD coating was facilely formed on Mg surface.

Supplementary data related to this article can be found at https://doi.org/10.1016/j.bioactmat.2020.07.019.

3.2. Electrochemical corrosion behavior

Fig. 3(a) shows the anodic and cathodic PDP curves of the uncoated and coated Mg plates in Hank's and NS solutions, and the electrochemical corrosion parameters from PDP curves are listed in Fig. 3(b) and Table S1. The corrosion current density (i_{corr}) is a kinetic parameter to evaluate corrosion resistance, while the corrosion potential (E_{corr}) is a thermodynamic parameter to estimate corrosion tendency [39]. E_{corr}
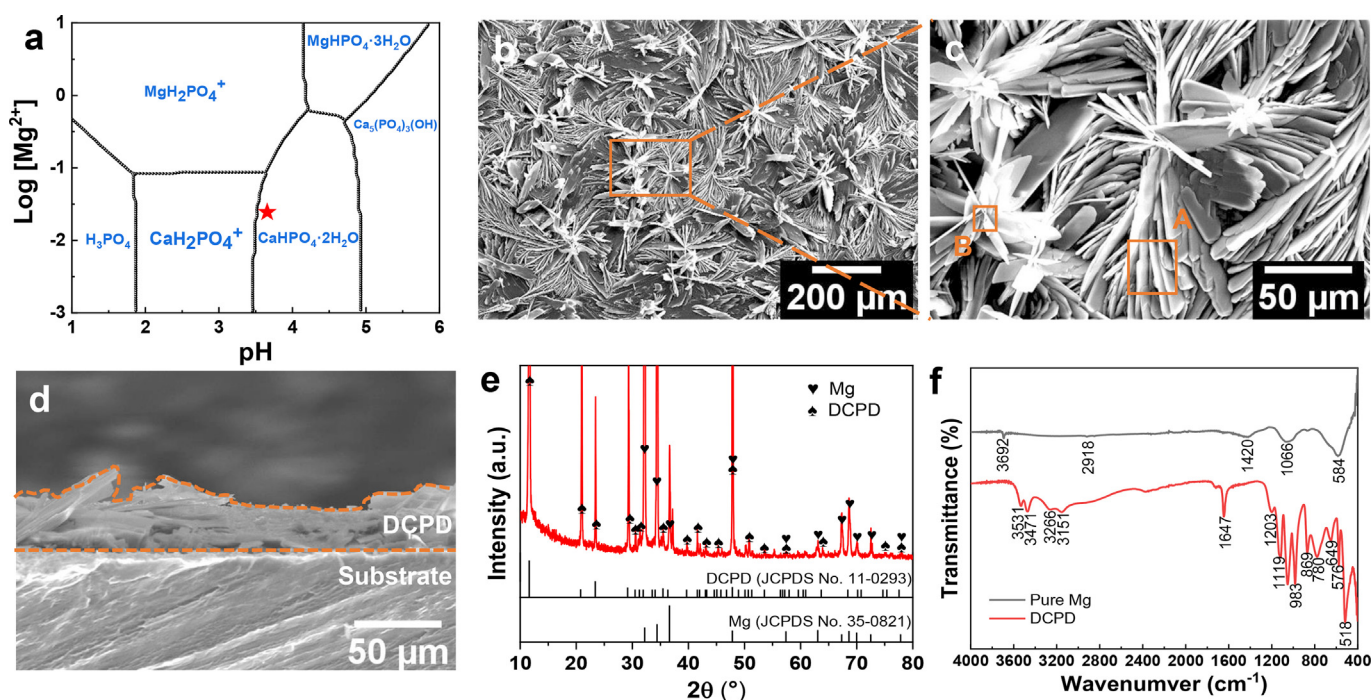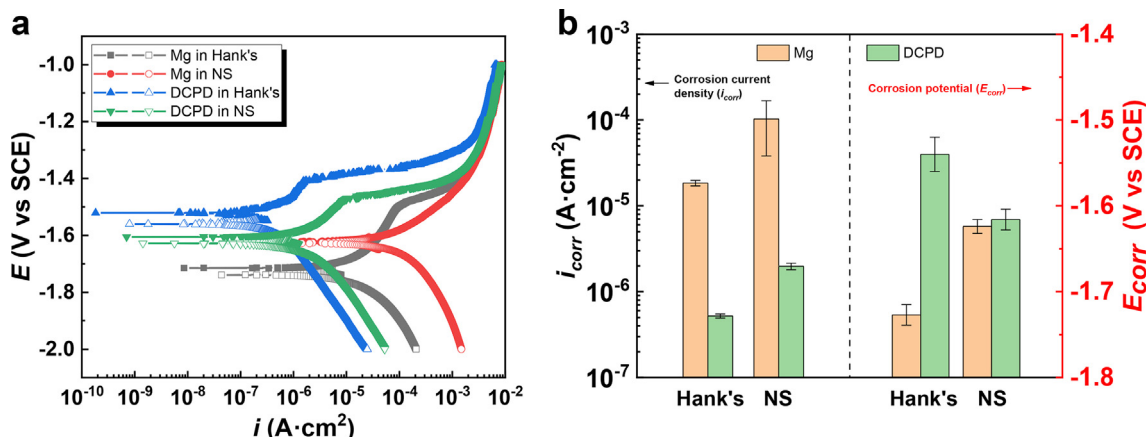

Fig. 2. Coating characterizations: (a) predominance area diagram calculated by MEDUSA software package [33], (b–d) surface and cross-section SEM morphologies, (e) XRD patterns, (f) FTIR spectra (A,B are the labels of the selected regions for EDS analysis in Fig. S3).

Fig. 3. Typical PDP curves of the DCPD uncoated and coated Mg plates in Hank's and NS solutions (a) and the relative electrochemical corrosion parameters (b) (In Fig. 3(a), the anodic branch is composed of the filled dots while the cathodic branch consists of the hollow dots).

increases to -1.54V vs SCE and i_{corr} decreases to 5.21×10^{-7} A·cm^{-2} when DCPD-coated Mg is immersed in Hank's solution. Besides, when immersed in NS solution, the coated sample exhibits an E_{corr} of -1.62V vs SCE and an i_{corr} of 1.98×10^{-6} A cm^{-2}. The DCPD-coated Mg plates exhibit a low tendency toward corrosion and good corrosion resistance in Hank's and NS solutions.

These common electrochemical corrosion methods are introduced to measure corrosion resistance, which might cause coating failures artificially, especially in PDP measurements. Besides, these methods cannot monitor and visualize the in-situ evolution of local corrosion behavior. Hence, SVET 3D mappings of the current density measured above DCPD-coated samples containing the scratch region are displayed in Fig. 4. Herein, SVET reflects ionic fluxes from corrosion activity [16], and red regions are detected as local corrosion. Because of the scratches, the uncoated Mg substrate is directly exposed to physiological environments. In the initial immersion stage, there are serious local corrosion behaviors in the scratch regions in both Hank's and NS solutions. With the immersion time extending to 1 h, the local corrosion is slightly slowed down. Herein, the scratched DCPD coated sample in Hank's solution exhibits relatively uniform corrosion behavior after immersed for 2 h in Hank's solution. However, a slight local corrosion behavior is still detected until the scratched DCPD coated sample is immersed in NS solution for 4 h. The SVET results exhibit the self-healing capability in Hank's and NS solutions. To confirm self-healing behavior, the scratch morphologies after immersed for 4 h are displayed in Fig. 5. The scratches are sealed by Ca,P-containing products detected by EDS analysis in Fig. 5, and the scratched coatings are self-healed in Hank's and NS solutions. By comparison, self-healing behavior in Hank's solution is more high-efficiency than that in NS solution, which might be attributed to inhibitor ions in Hank's solution (for example, phosphate ions [17,22]).

Fig. 6 shows EIS results of the bare and coated Mg plates in Hank's and NS solutions (The points represent the experimental data while the lines display the fitting results). The frequency-phase bode plots (in Fig. 6(c,f)) show two time constants for pure Mg and DCPD coating in Hank's or NS solution, and three time constants for the scratched DCPD coating in NS solution. Based on the time constants (in Fig. 6(c,f)) and coating structure (in Fig. 2(d)), EIS results were fitted with these equivalent circuit models in Fig. 6(g–i), and the fitting equivalent circuit parameters are listed in Table S2. In these equivalent circuit models, R_s is the solution resistance, DCPD coating and surface oxide film are related to a coating resistance (R_c) (virtual pore resistance) paralleled with a constant phase element (Q_c), and substrate-coating interface reaction is represented by the charge transfer resistance (R_{ct})
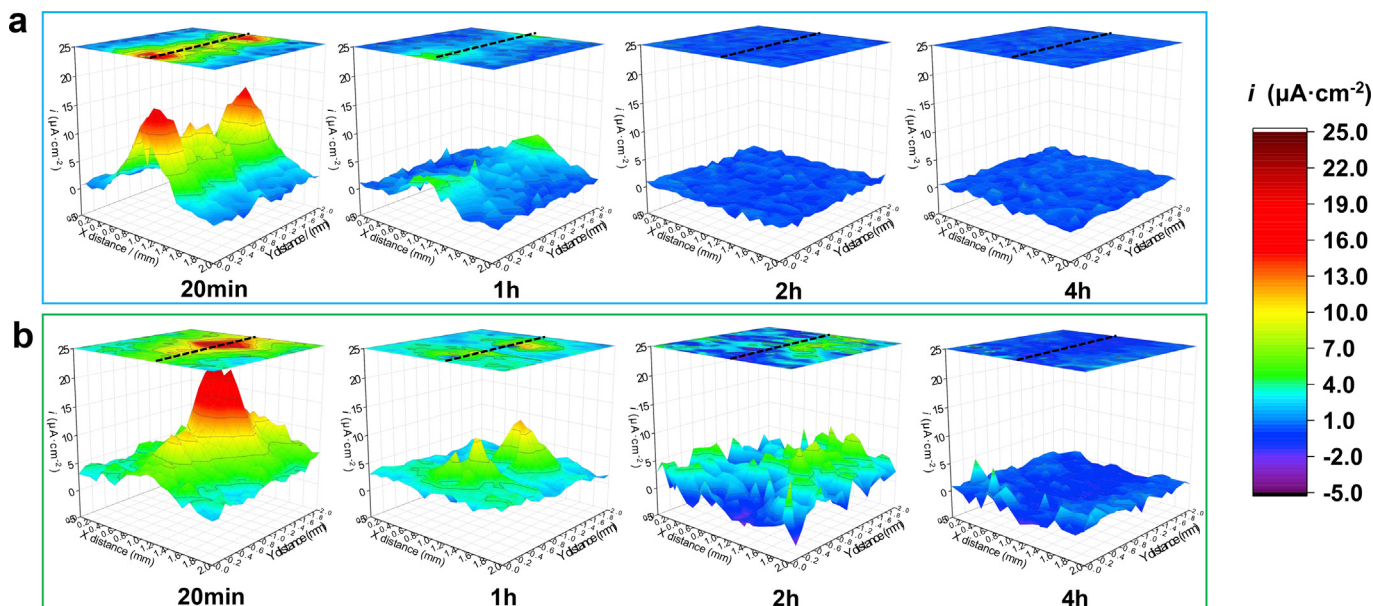
Fig. 4. SVET 3D mappings of the scratch region immersed in Hank's (a) and NS (b) solutions (Black dotted line indicates scratch location).
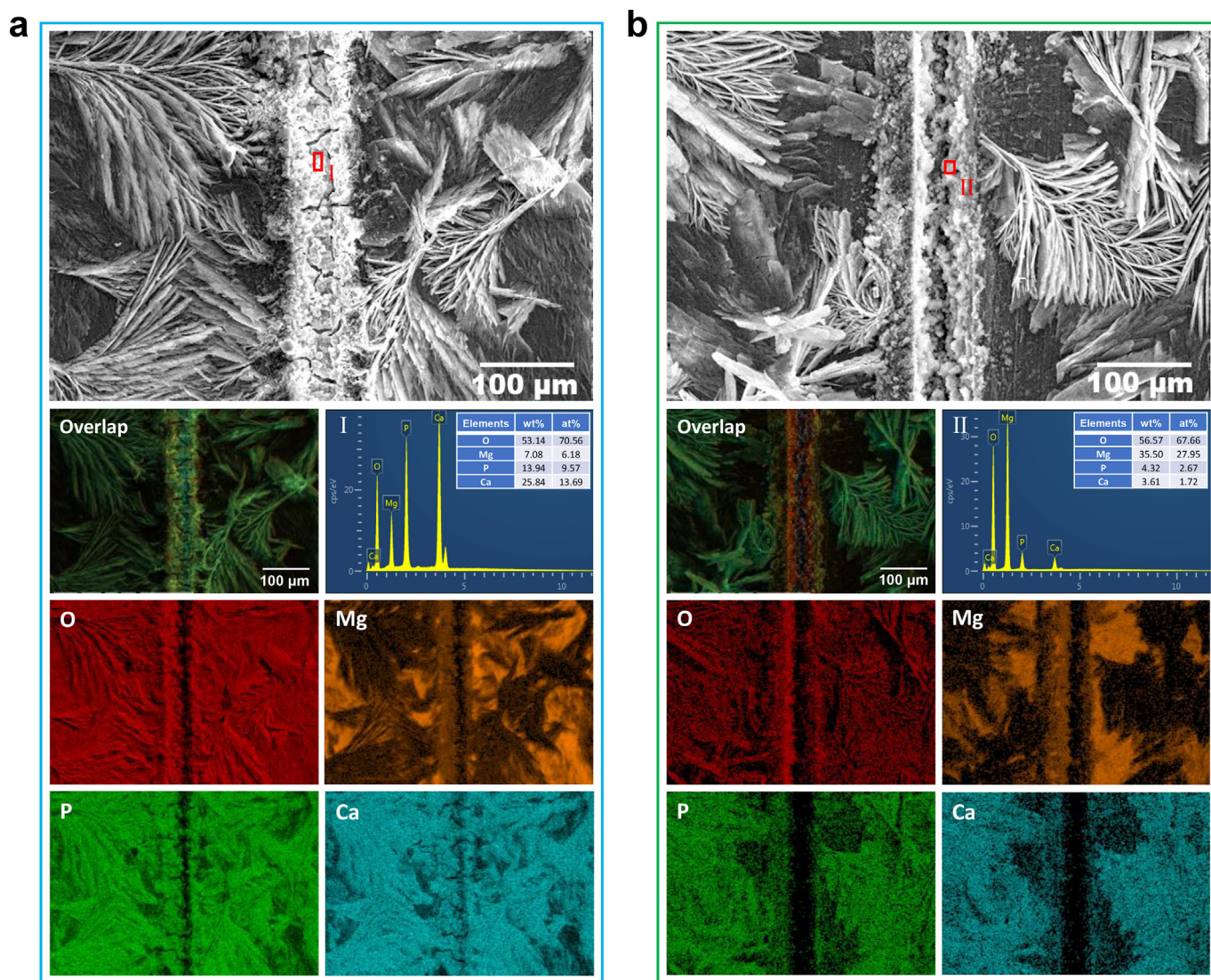
Fig. 5. The scratch morphologies after immersed for 4 h in Hank's (a) and NS (b) solutions, and corresponding EDS mappings of overlap, O, Mg, P and Ca elements as well as EDS spectra of the selected regions.

paralleled with a double-layer constant phase element (Q_{dl}). Besides, the inductive behavior is corresponding to the resistance (R_L) in series with an inductance (L), indicating the initiation of pitting corrosion [40]. EIS plots for Mg plates in Hank's and NS solutions consist of similar capacitive loops, which can be fitted by the equivalent circuit model in Fig. 6(g). EIS results for the scratched DCPD coated Mg at the initial immersion stage are unstable at the low-frequency region, which is attributed to the serious interface reaction in the scratches. When the scratched DCPD coated Mg is immersed in NS solution, the inductive behavior appears owing to local corrosion behavior, thus the EIS results are fitted with the equivalent circuit model in Fig. 6(i). With prolonging the immersion time, the inductive component disappears, the capacitive loop becomes larger, and then EIS plots are well-fitted with the equivalent circuit model in Fig. 6(h). Generally, a larger capacitive loop represents a better corrosion resistance [41], which is corresponded to a larger low-frequency modulus impedance ($|Z|_{0.1Hz}$) in Fig. 6(b,e). When the scratched DCPD was immersed for 4 h, $|Z|_{0.1Hz}$ increases from 26390 Ω cm^2 to 31600 Ω cm^2 in Hank's solution, which reaches 82.7% $|Z|_{0.1Hz}$ of untreated DCPD coating sample. Besides, $|Z|_{0.1Hz}$ increases from 5695 Ω cm^2 to 13460 Ω cm^2 in NS solution, which is 46.8% $|Z|_{0.1Hz}$ of untreated DCPD coating sample. Besides, the increase in phase angle in the low-frequency region (Fig. 6(c,f)) indicates that a highly dense film with fewer cracks is formed with the extension of

immersion time [42]. The change in EIS results proves that DCPD coating can realize self-healing to offer protection for Mg in physiological environments. Herein, Hank's solution promotes the self-healing behavior of DCPD. By contrast, DCPD displays efficient self-healing ability than OCP and HA [12].

3.3. In-vitro degradation behavior

Long-time immersion experiments were introduced to further reveal the degradation behavior of the uncoated and coated Mg in Hank's and NS solutions. Hydrogen evolution is accompanied by the dissolution of metallic Mg, as summarized in Equation (2-4) [43,44].

$$Mg \rightarrow Mg^{2+} + 2e^- \tag{2}$$

$$2H_2O + 2e^- \rightarrow H_2(g) + 2OH^- \tag{3}$$

$$Mg + 2H_2O \rightarrow Mg(OH)_2 + H_2 \tag{4}$$

Fig. 7 displays the hydrogen evolution and corresponding corrosion rate curves of DCPD coated and uncoated Mg plates in Hank's and NS solutions. The uncoated Mg plates are corroded seriously, especially in the NS solution (Fig. 7(b)). Hank's solution contains a great deal of inhibiting ions, such as phosphate, which would slow down the
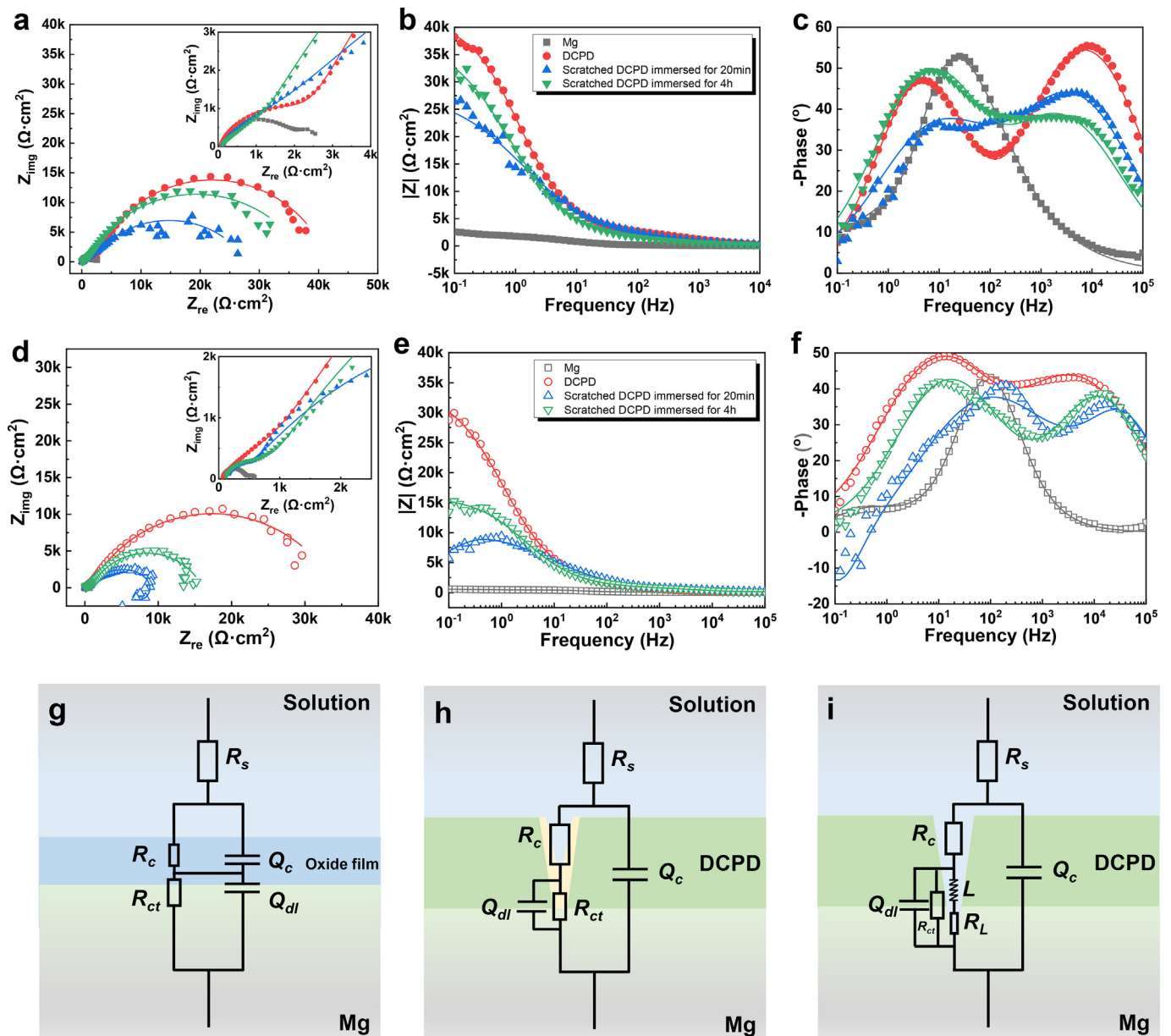
Fig. 6. Typical EIS results of DCPD coated and uncoated Mg plates immersed in Hank's solution (a–c) and NS solution (d–f), and relevant equivalent circuit models (g–i) (EIS plots for Mg in Hank's or NS solution are fitted by Model (g); EIS plots for DCPD in Hank's or NS solution are fitted with Model (h); EIS plots for the scratched DCPD in NS solution are fitted with Model (i)).

degradation of Mg plates [17,22]. The corresponding corrosion rate was calculated based on hydrogen evolution curves according to Equation (5) [45]:

$$P_H = 54.696 \, \nu_H \tag{5}$$

Where P_H is the corrosion rate of Mg (mm·y^{-1}). And ν_H is the hydrogen evolution rate (mL·cm^{-2}·h^{-1}) obtained from hydrogen evolution curves by the Origin program. Fig. 7(c and d) display the corresponding corrosion rate in Hank's and NS solutions. When pure Mg is exposed without any barriers in the corrosive solutions, thus the hydrogen evolution rate is rapid at the initial immersion stage. With the extension of the immersion period, the hydrogen evolution rate is slightly decreased. In this stage, the corrosion products are formed to protect Mg plates against rapid corrosion. When pure Mg is immersed in Hank's solution, a temporary increase in the corrosion rate appears in Fig. 7(c), which is attributed to the formation and breakdown of the corrosion product layer on Mg [46]. But a temporary increase in corrosion rate

cannot be found in NS solution (Fig. 7(d)), because corrosion products are hardly covered on Mg to slow down the corrosion rate. Besides, the in-vitro immersion behaviors of scratched DCPD coatings are evaluated to investigate the self-healing capability. In Fig. 7, the scratched DCPD-coated sample releases slightly more hydrogen than the unscratched one, but also provide good protection for Mg. With the immersion time increasing, there are no obvious differences in overall corrosion rate between unscratched and scratched DCPD-coated samples, implying that DCPD coatings are equipped with self-healing capacity in physiological solutions, and local corrosion from coating damages has a limited effect on hydrogen evolution.

4. Discussion

4.1. Self-healing behavior

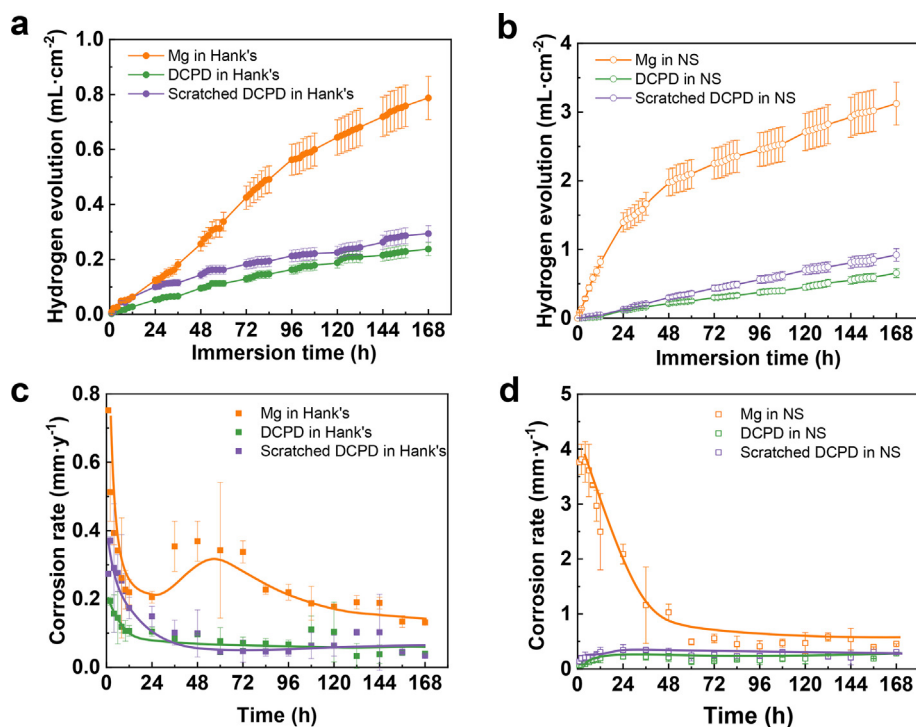Fig. 8 shows the surface morphologies and the corresponding EDS

Fig. 7. Hydrogen evolution curves (a,b) and corresponding corrosion rate (c,d) as a function of immersion time.

mappings of unscratched and scratched DCPD-coated samples after immersed for 7 days. Besides, the surface morphologies of bare Mg after 7-day immersion are provided in Fig. S4. After immersion, the coatings remain needle-shape in Fig. 8(a and b), but it could be found that many obvious micro-cracks appear in needle-shaped coatings, especially in NS solutions. The corresponding chemical composition results are listed in Fig. S3. The immersed coatings are composed of O, Mg, P, and Ca elements as well as few Na and Cl elements. The scratches are covered with corrosion products, which is the reason to realize self-healing. The corrosion products on the scratch are mainly composed of O, P, Mg, and

Ca elements. However, Ca/P ratio (at. %) on surfaces or scratches is located at a wide range from 0.67 to 1.58 as shown in Fig. S3, thus the phase composition of Ca,P-riched compounds is unconfirmed. In Fig. 8(e–f), it seems that O element is preferably along with Mg element, while Ca element tends to be accompanied with P element around the scratches, inferring that the corrosion products in the scratch contain $Mg(OH)_2$ (in Equation (4)) and Ca,P-riched compounds. Remarkably, a lower content of Ca and P elements are determined on the scratch immersed in NS solution, attributed to a difference in chemical composition between Hank's and NS solutions. Hank's solution
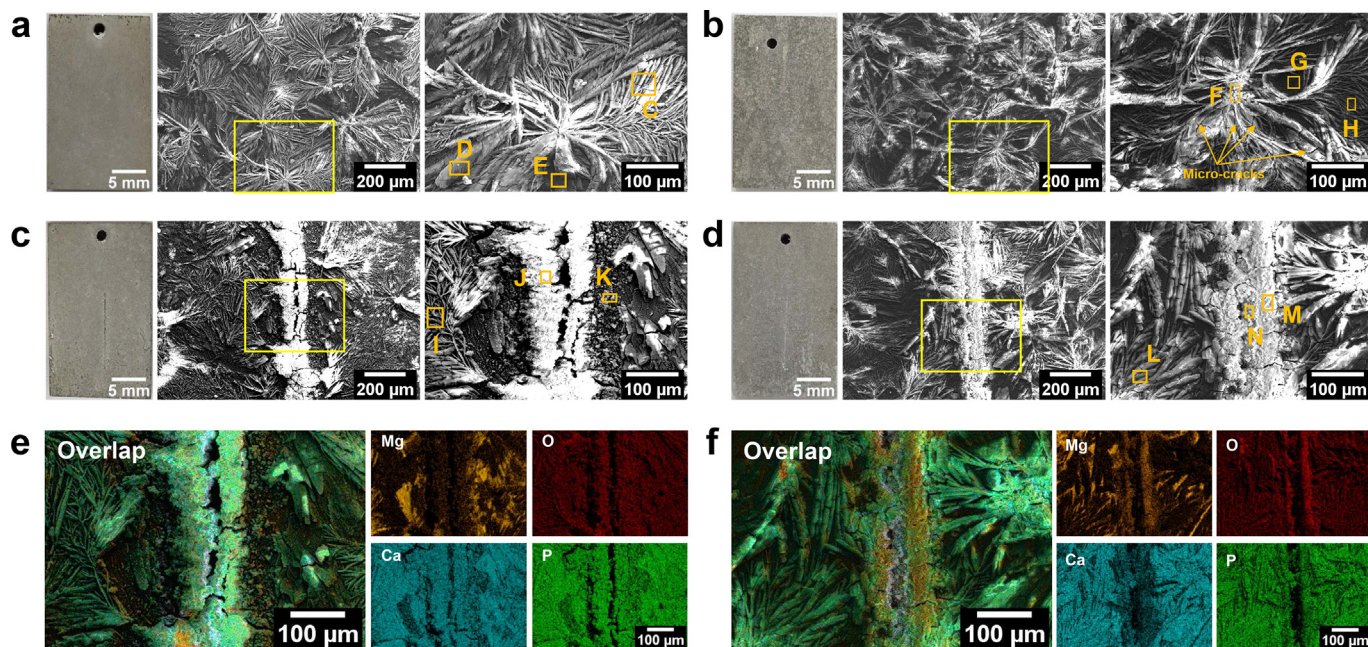

Fig. 8. Surface morphologies after immersion of 7 days: (a) the coating in Hank's, (b) the coating in NS, (c) the scratched coating in Hank's, (d) the scratched coating in NS, and the corresponding EDS mappings of overlap, Mg, O, Ca and P elements ((e) corresponds to (c), and (f) is matched with (d); Regions C-M are corresponding to the selected regions for EDS analysis in Fig. S3).
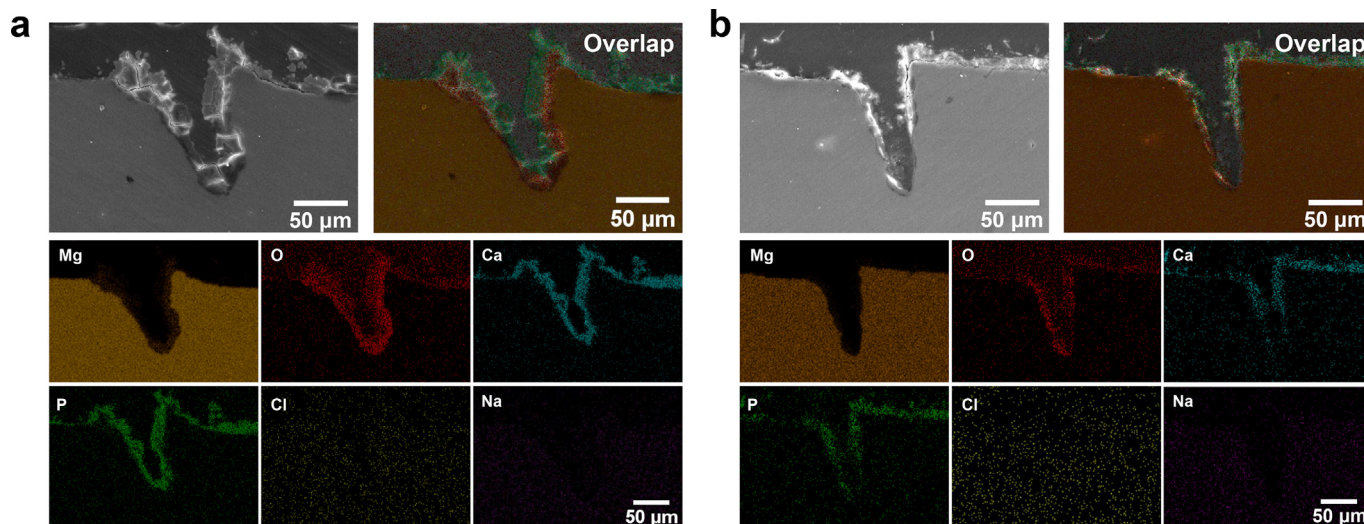
Fig. 9. Cross-section morphologies of the scratched coatings in Hank's (a) and NS (b) solutions, and EDS mappings of overlap, Mg, P, O, Ca, P, Cl and Na.

provides extra calcium and phosphate ions to form anti-corrosive compounds, which would promote self-healing behavior. However, calcium and phosphate ions are only originated from DCPD coatings in NS solution. The above phenomenon reflects that the self-healing can occur not only in Hank's solution but also in NS solution, but the related self-healing mechanisms are slightly different in two solutions.

In order to further investigate the self-healing behaviors in Hank's and NS solutions, the cross-section morphologies of the immersed samples are shown in Fig. 9. The scratches are sealed with corrosion products. Herein, the corrosion product layers are mainly composed of O, Mg, P and Ca elements. Besides, it is noticeable that the O-rich products are formed in advance of Ca,P-rich compounds. At the initial immersion stage, the uncovered Mg substrate is exposed to corrosive physiological solutions, and then dissolved along with the hydrogen evolution and the formation of the local alkaline environment. Subsequently, the $Mg(OH)_2$ layer is preferentially formed. In addition, DCPD coating is sensitive to the pH increase, and tends to dissolve and transform into other Ca–P compounds. $Mg(OH)_2$ film along with the Mg-contained Ca–P film is successively formed on the scratch so that an anti-corrosive composite film retards a further pitting corrosion in scratches. By contrast, the corrosion product layer in Hank's solution seems thicker than that in NS solution, as exhibited in Fig. 9. P and Ca elements from DCPD are limited while Ca and P elements in Hank's solution are supplied for the formation of the anti-corrosion layer in scratches, leading to the differences in self-healing behavior.

4.2. Self-healing mechanism

In order to reveal the self-healing mechanism of DCPD, the immersed coatings were characterized in detail. FTIR spectra, the XRD patterns and TEM morphologies are shown in Fig. 10. FTIR spectra are displayed in Fig. 10(a), in which the two peaks at 3166 cm^{-2} and 3216 cm^{-2} are related to O–H stretching modes in H_2O. Besides, the internal phosphate (PO_4^{3-}) group are characterized based on ν_1 (PO_4^{3-}) symmetric stretching, ν_2 (PO_4^{3-}) out-of-plane bending, ν_3 (PO_4^{3-}) asymmetric stretching modes and ν_4 (PO_4^{3-}) in-plane bending [38]. Also, the XRD patterns are characterized to further study the phase transformation, as shown in Fig. 10(b). The X-ray diffraction peaks of DCPD can be still detected in the DCPD-coated sample after 7d immersion in Hank's solution, but disappear after immersed in NS solution for 7d, implying that NS solution is more aggressive to DCPD coating than Hank's solution. Compared with untreated DCPD coating, many broad X-ray diffuse peaks are attributed to corresponding to HA (JCPDS No.09–0432) and its amorphous state, as observed in Fig. 10(b).

Moreover, TEM images and selected area electron diffraction (SEAD) patterns are shown in Fig. 10(c and d). After immersion tests, the SAED patterns display a diffused halo ring related to amorphous structure [47,48]. Thus, the results from XRD, FTIR, and TEM reveal the phase transformation from DCPD to amorphous calcium phosphate (ACP) and HA. In many previous findings [47,48], Mg^{2+} ions are reported as vital factors that inhibit spontaneous HA crystallization. In our work, Mg^{2+} ions release into solutions owing to biodegradability. It is found that Mg ions are surface-absorbed and/or incorporated into Ca–P compounds (in Figs. 8 and 9), resulting in the inhibiting of HA crystallization and the formation of ACP compound [49]. ACP has been regarded as a significant constituent bone tissue mineral [50], and reported to have a better osteoconduction property than other forms of Ca–P compounds [51]. DCPD and its products in physiological solutions would provide favorable protection and biocompatibility for biodegradable Mg implants.

Furthermore, the greater solubility of DCPD is induced by pH sensitivity, which provides the possibility for self-healing. Generally, DCPD is considered as a precursor to other forms of Ca–P phases, especially in alkaline environments [25]. To reveal the Ca–P phase transformation in physiological environments, the thermodynamic driving forces for various Ca–P compounds were analyzed based on the ΔG as a function of pH in physiological solutions. Fig. 11(a) illustrates the correlation curves of ΔG as a function of pH calculated using the PHREEQC program [32]. The original DCPD coatings on pure Mg are unstable and tend to be dissolved out of pH range from 7.6 to 8.2 in Hank's solution as well as from 7.8 to 8.0 in NS solution. It seems that DCPD in Hank's solution is more stable than that in NS solution when located in a wide pH range, leading to remained DCPD phase after 7d immersion in Hank's solution, as detected in Fig. 10(b). Whereas HA exhibits a larger thermodynamic driving force than other forms of Ca–P compounds in physiological solutions. When DCPD coating is scratched, the exposed Mg substrate is rapidly degraded so that the local alkalinity is generated near the scratch. The local alkalinity might accelerate the dissolution of DCPD and the formation of other Ca–P compounds, which contributes to the self-healing capacity. Besides, ICP results in Fig. 11(b) show that the released Ca and P ion concentration is different at various pH. With the pH increase from 7.4 to 10.0, the Ca and P ion concentration gradually slows down. During immersion, the dissolution of DCPD is along with the formation of other Ca–P compounds, and what makes differences is attributed to the differences from the association/dissociation reaction rate of Ca–P compounds at various pH. Ca^{2+} and PO_4^{3-} ions are dissolved from DCPD, and then precipitated back to the surface as other forms of Ca–P compounds. An interesting point to consider is that
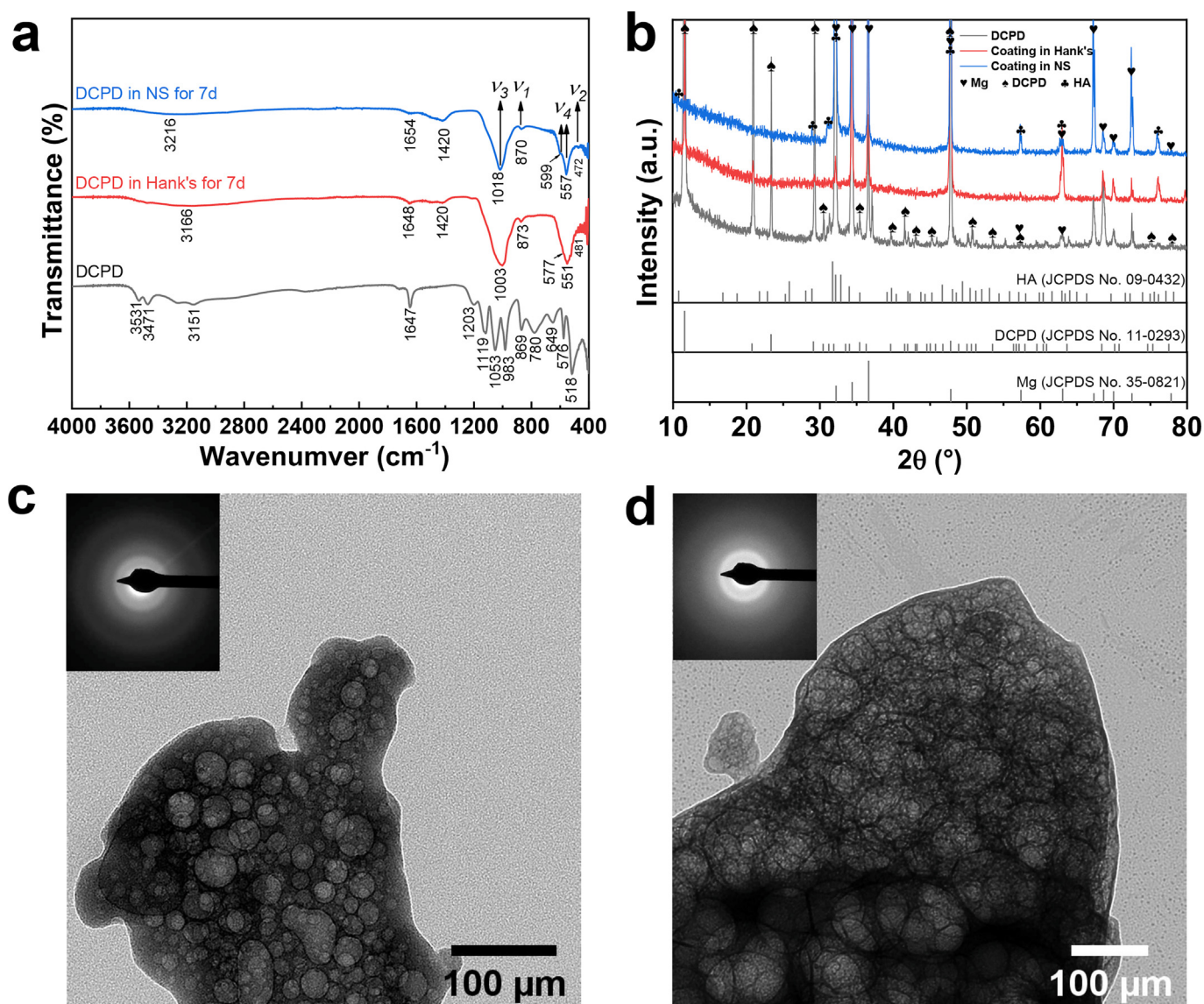
Fig. 10. Characterizations of coatings after immersion in Hank's or NS solutions: FTIR spectra (a), XRD patterns (b) and TEM morphologies ((c) in Hank's and (d) in NS).
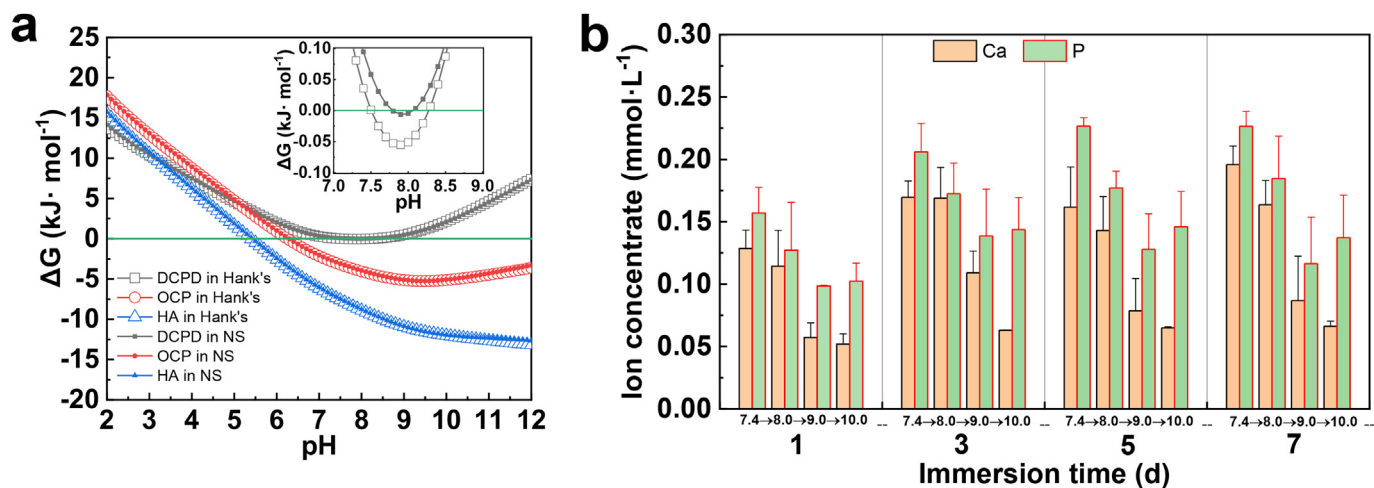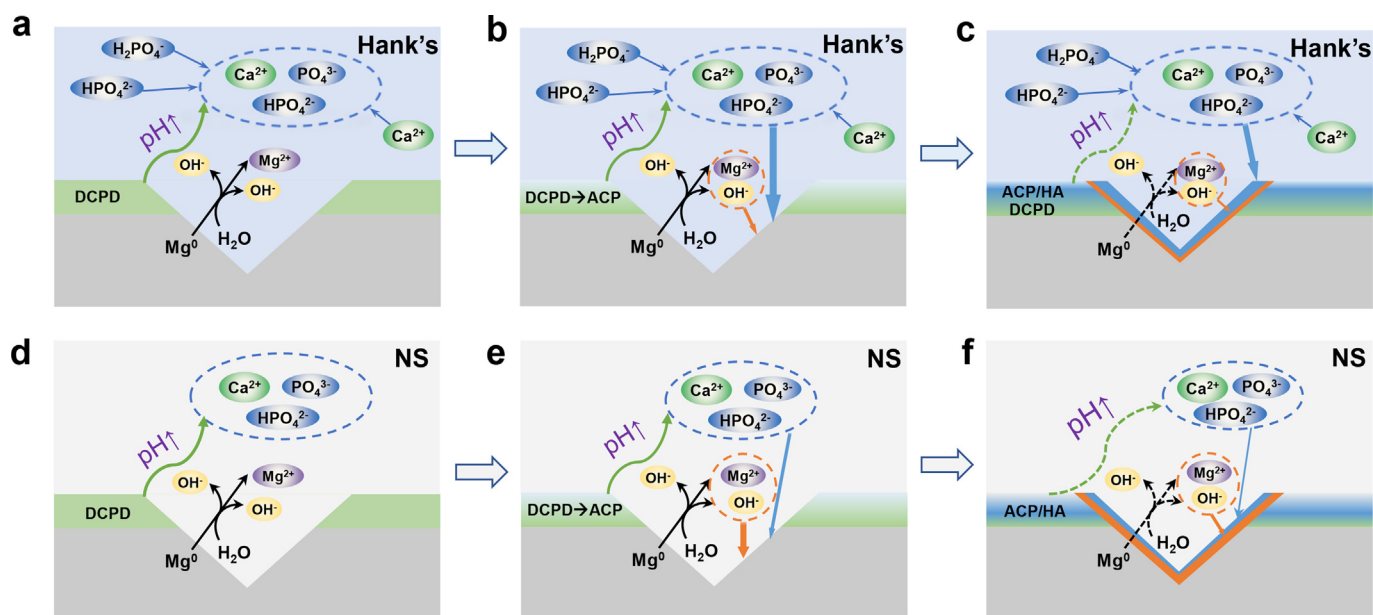

Fig. 11. (a) Correlation curves of ΔG as a function of pH for Ca–P compounds in Hank's or NS solutions, (b) Ca and P ion concentrations in the multi-pH deionized water solutions.

Fig. 12. Self-healing schematic diagrams of scratched DCPD coatings in Hank's (a–c) and NS (d–f) solutions (DCPD: dicalcium phosphate dihydrate coating; ACP: amorphous calcium phosphate; HA: hydroxyapatite).

Ca/P ratio is less than 1, especially at pH = 10.0. In other words, the Ca/P ratio in the immersed coating is more than 1, especially at alkaline conditions. The greater solubility induced by pH sensitivity might endow DCPD with more advantages in self-healing efficiency than HA and OCP [12].

In conclusion, the self-healing behaviors in Hank's and NS solutions have both similarities and differences, as illustrated in Fig. 12. When the coating is scratched, the exposed Mg substrate is corroded preferentially, meanwhile local alkalinity is formed in these scratches, as demonstrated in Equation (2,3). Owing to local alkalinity, DCPD crystals tend to dissolve and release calcium and phosphate ions near the scratches as illustrated in Fig. 12(a,d). With the further increase in local pH, $Mg(OH)_2$ and Mg-containing Ca–P compounds are successively formed in the scratches (in Fig. 12(b,e)), and thereby the scratches are sealed to realize self-healing (in Fig. 12(c,f)). On the one hand, DCPD provides film-formation ions to retard local corrosion, which is deemed as an autonomous self-healing mechanism [13]. On the other hand, the corrosion inhibitors and film-formation ions in Hank's solutions can be able to enhance the self-healing capacity (in Fig. 12(d–f)), indicating autonomous self-healing capacity enhanced with foreign-aid corrosion inhibitors.

Generally, self-healing coatings are composed of two parts: a "host" as a physical barrier as well as a corrosion inhibitor carrier, and a "guest" as a corrosion inhibitor [13,21]. Zhao et al. [20] reported self-healing multilayer film capsuled with SiO_2 and CeO_2 nanoparticles, in which SiO_2 was a "host" while CeO_2 was "guest". Moreover, Xiong et al. [21,22] introduced silk fibroin as "host" and K_3PO_4/phytic acid as "guest" to self-healing coatings for biodegradable Mg. In brief, compositing and multilayering are common methods to integrate "host" with "guest" into self-healing coatings. However, in our present work, a single DCPD coating also exhibits self-healing ability, and the self-healing coating is facilely prepared on biodegradable Mg without compositing or multilayering. Thus, the DCPD coating also consists of "host" and "guest", but DCPD is acted as not only a "host" but also a "guest", indicating the autonomous self-healing without extra corrosion inhibitors embedded in the coating. Moreover, DCPD has a higher supplement for Ca^{2+} and PO_4^{3-} ions to realize more efficient self-healing capability than OCP and HA [12]. When local corrosion occurs in the coating failure, a local alkaline environment is formed in the failure region. Based on the correlation curves of ΔG as a function of pH

(in Fig. 11(a)), the pH increase can stimulate the releasing of calcium and phosphate ions from DCPD, but inhibit the dissolution of HA and OCP. In conclusion, DCPD coating with self-healing capacity demonstrates many noteworthy features in preparation method and self-healing mechanism, which would promote wide applications of DCPD on Mg implants, and open new opportunities to further explore self-healing coatings of biodegradable Mg for clinical applications.

5. Conclusion

In this works, DCPD coatings were fabricated on pure Mg plates via a facile preparation method. The electrochemical corrosion measurements and in vitro immersion experiments indicated that DCPD coatings not only provided good corrosion control for biodegradable Mg but also exhibited self-healing ability in both Hank's and NS solutions. Local alkaline from scratches promoted the formation of anti-corrosive product layers owing to the supplement of Ca and P from DCPD, resulting in the scratch sealing to realize autonomous self-healing without embedding extra corrosion inhibitors in DCPD. In this self-healing system, DCPD was acted as not only a physical barrier but also a self-healing agent. Besides, Hank's solution could provide foreign-aid corrosion inhibitors to promote autonomous self-healing. The research findings provide an insight into self-healing capacity of facilely prepared DCPD coatings on pure Mg, and open new opportunities to further explore of efficient self-healing coatings on bio-Mg implants.

CRediT authorship contribution statement

Qiangsheng Dong: Conceptualization, Methodology, Writing - original draft. **Xingxing Zhou:** Methodology, Investigation. **Yuanjia Feng:** Methodology, Validation. **Kun Qian:** Methodology, Formal analysis. **Huan Liu:** Investigation, Formal analysis. **Mengmeng Lu:** Investigation. **Chenglin Chu:** Resources, Funding acquisition. **Feng Xue:** Conceptualization, Supervision, Funding acquisition. **Jing Bai:** Conceptualization, Visualization, Writing - review & editing.

Declaration of competing interest

The authors declare no conflict of interest.

Acknowledgments

Appendix A. Supplementary data

Supplementary data to this article can be found online at https://doi.org/10.1016/j.bioactmat.2020.07.019.

References

[1] Y.F. Zheng, X.N. Gu, F. Witte, Biodegradable metals, Mat. Sci. Eng. R 77 (2014) 1–34.
[2] G.L. Song, S.Z. Song, A possible biodegradable magnesium implant material, Adv. Eng. Mater. 9 (4) (2007) 298–302.
[3] Y. Sun, H.L. Wu, W.H. Wang, R. Zan, H.Z. Peng, S.X. Zhang, X.N. Zhang, Translational status of biomedical Mg devices in China, Bioact. Mater. 4 (2019) 358–365.
[4] M.S. Song, R.C. Zeng, Y.F. Ding, R.W. Li, M. Easton, I. Cole, N. Birbilis, X.B. Chen, Recent advances in biodegradation controls over Mg alloys for bone fracture management: a review, J. Mater. Sci. Technol. 35 (4) (2019) 535–544.
[5] R.F. Li, L. Wang, D.Y. Kong, L. Yin, Recent progress on biodegradable materials and transient electronics, Bioact. Mater. 3 (3) (2018) 322–333.
[6] G.L. Song, Control of biodegradation of biocompatable magnesium alloys, Corrosion Sci. 49 (4) (2007) 1696–1701.
[7] T.S.N.S. Narayanan, I.S. Park, M.H. Lee, Strategies to improve the corrosion resistance of microarc oxidation (MAO) coated magnesium alloys for degradable implants: prospects and challenges, Prog. Mater. Sci. 60 (2014) 1–71.
[8] L.Y. Cui, S.C. Cheng, L.X. Liang, J.C. Zhang, S.Q. Li, Z.L. Wang, R.C. Zeng, In vitro corrosion resistance of layer-by-layer assembled polyacrylic acid multilayers induced Ca-P coating on magnesium alloy AZ31, Bioact. Mater. 5 (1) (2020) 153–163.
[9] L.Y. Li, L.Y. Cui, R.C. Zeng, S.Q. Li, X.B. Chen, Y.F. Zheng, M.B. Kannan, Advances in functionalized polymer coatings on biodegradable magnesium alloys - a review, Acta Biomater. 79 (2018) 23–36.
[10] Z.Z. Yin, W.C. Qi, R.C. Zeng, X.B. Chen, C.D. Gu, S.K. Guan, Y.F. Zheng, Advances in coatings on biodegradable magnesium alloys, J. Magnes. Alloy. 8 (1) (2020) 42–65.
[11] L. Huang, J. Li, W. Yuan, X.M. Liu, Z.Y. Li, Y.F. Zheng, Y.Q. Liang, S.L. Zhu, Z.D. Cui, X.J. Yang, K.W.K. Yeung, S.L. Wu, Near-infrared light controlled fast self-healing protective coating on magnesium alloy, Corrosion Sci. 163 (2020) 108257.
[12] S. Hiromoto, Self-healing property of hydroxyapatite and octacalcium phosphate coatings on pure magnesium and magnesium alloy, Corrosion Sci. 100 (2015) 284–294.
[13] F. Zhang, P.F. Ju, M.Q. Pan, D.W. Zhang, Y. Huang, G.L. Li, X.G. Li, Self-healing mechanisms in smart protective coatings: a review, Corrosion Sci. 144 (2018) 74–88.
[14] Z.H. Xie, D. Li, Z. Skeete, A. Sharma, C.J. Zhong, Nanocontainer-enhanced self-healing for corrosion-resistant Ni coating on Mg alloy, ACS Appl. Mater. Interfaces 9 (41) (2017) 36247–36260.
[15] F. Fan, C.Y. Zhou, X. Wang, J. Szpunar, Layer-by-Layer assembly of a self-healing anticorrosion coating on magnesium alloys, ACS Appl. Mater. Interfaces 7 (49) (2015) 27271–27278.
[16] L.M. Calado, M.G. Taryba, M.J. Carmezim, F. Montemor, Self-healing ceria-modified coating for corrosion protection of AZ31 magnesium alloy, Corrosion Sci. 142 (2018) 12–21.
[17] D. Liu, E.H. Han, Y.W. Song, D.Y. Shan, Enhancing the self-healing property by adding the synergetic corrosion inhibitors of Na3PO4 and 2-mercaptobenzothiazole into the coating of Mg alloy, Electrochim. Acta 323 (2019) 134796.
[18] X. Wang, L.X. Li, Z.H. Xie, G. Yu, Duplex coating combining layered double hydroxide and 8-quinolinol layers on Mg alloy for corrosion protection, Electrochim. Acta 283 (2018) 1845–1857.
[19] J.L. Chen, L. Fang, F. Wu, J. Xie, J. Hu, B. Jiang, H.J. Luo, Corrosion resistance of a self-healing rose-like MgAl-LDH coating intercalated with aspartic acid on AZ31 Mg alloy, Prog. Org. Coating 136 (2019) 105234.
[20] Y.B. Zhao, Z. Zhang, L.Q. Shi, F. Zhang, S.Q. Li, R.C. Zeng, Corrosion resistance of a self-healing multilayer film based on SiO2 and CeO2 nanoparticles layer-by-layer assembly on Mg alloys, Mater. Lett. 237 (2019) 14–18.
[21] P. Xiong, Z.J. Jia, W.H. Zhou, J.L. Yan, P. Wang, W. Yuan, Y.Y. Li, Y. Cheng, Z.P. Guan, Y.F. Zheng, Osteogenic and pH stimuli-responsive self-healing coating on biomedical Mg-1Ca alloy, Acta Biomater. 92 (2019) 336–350.
[22] P. Xiong, J.L. Yan, P. Wang, Z.J. Jia, W.H. Zhou, W. Yuan, Y.Y. Li, Y. Liu, Y. Cheng, D.F. Chen, Y.F. Zheng, A pH-sensitive self-healing coating for biodegradable magnesium implants, Acta Biomater. 98 (2019) 160–173.
[23] B. Liu, X. Zhang, G.Y. Xiao, Y.P. Lu, Phosphate chemical conversion coatings on metallic substrates for biomedical application: a review, Mater. Sci. Eng. C 47 (2015) 97–104.
[24] Y.C. Su, I. Cockerill, Y.F. Zheng, L.P. Tang, Y.X. Qin, D.H. Zhu, Biofunctionalization of metallic implants by calcium phosphate coatings, Bioact. Mater. 4 (2019) 196–206.
[25] M. Kumar, H. Dasarathy, C. Riley, Electrodeposition of brushite coatings and their transformation to hydroxyapatite in aqueous solutions, J. Biomed. Mater. Res. 45 (4) (1999) 302–310.
[26] M.B. Kannan, Electrochemical deposition of calcium phosphates on magnesium and its alloys for improved biodegradation performance: a review, Surf. Coating. Technol. 301 (2016) 36–41.
[27] J.L. Niu, G.Y. Yuan, Y. Liao, L. Mao, J. Zhang, Y.P. Wang, F. Huang, Y. Jiang, Y.H. He, W.J. Ding, Enhanced biocorrosion resistance and biocompatibility of degradable Mg-Nd-Zn-Zr alloy by brushite coating, Mater. Sci. Eng. C 33 (8) (2013) 4833–4841.
[28] C.Y. Li, C. Yu, R.C. Zeng, B.C. Zhang, L.Y. Cui, J. Wan, Y. Xia, In vitro corrosion resistance of a Ta2O5 nanofilm on MAO coated magnesium alloy AZ31 by atomic layer deposition, Bioact. Mater. 5 (1) (2020) 34–43.
[29] L.Y. Han, X. Li, J. Bai, F. Xue, Y.F. Zheng, C.L. Chu, Effects of flow velocity and different corrosion media on the in vitro bio-corrosion behaviors of AZ31 magnesium alloy, Mater. Chem. Phys. 217 (2018) 300–307.
[30] A.E. Somers, B.R.W. Hinton, C. de Bruin-Dickason, G.B. Deacon, P.C. Junk, M. Forsyth, New, environmentally friendly, rare earth carboxylate corrosion inhibitors for mild steel, Corrosion Sci. 139 (2018) 430–437.
[31] D. Snihirova, S.V. Lamaka, Y. Gonzalez-Garcia, A. Yilmaz, N. Scharnagl, M.F. Montemor, M.L. Zheludkevich, Influence of inhibitor adsorption on readings of microelectrode during SVET measurements, Electrochim. Acta 322 (2019) 134761.
[32] M. Laveissiere, H. Cerda, J. Roche, L. Cassayre, L. Arurault, In-depth study of the influence of electrolyte composition on coatings prepared by plasma electrolytic oxidation of TA6V alloy, Surf. Coating. Technol. 361 (2019) 50–62.
[33] Royal Institute of Technology, Chemical Equilibrium Diagrams, (2020) Sweden https://www.kemi.kth.se/medusa accessed 24 Feb 2020.
[34] X.B. Chen, N. Birbilis, T.B. Abbott, Effect of [Ca2+] and [PO43-] levels on the formation of calcium phosphate conversion coatings on die-cast magnesium alloy AZ91D, Corrosion Sci. 55 (2012) 226–232.
[35] Y.D. Li, W.Q. Wang, J.T. Duan, M. Qi, A super-hydrophilic coating with a macro/micro/nano triple hierarchical structure on titanium by two-step micro-arc oxidation treatment for biomedical applications, Surf. Coating. Technol. 311 (2017) 1–9.
[36] Y.Y. Zhu, G.M. Wu, Y.H. Zhang, Q. Zhao, Growth and characterization of Mg(OH)2 film on magnesium alloy AZ31, Appl. Surf. Sci. 257 (14) (2011) 6129–6137.
[37] A. Rafeek, G. Choi, L. Evans, Morphological, spectroscopic and crystallographic studies of calcium phosphate bioceramic powders, J. Australas. Ceram. Soc. 54 (1) (2018) 161–168.
[38] S. Turk, I. Altinsoy, G. CelebiEfe, M. Ipek, M. Ozacar, C. Bindal, Biomimetric coating of monophasic brushite on Ti6Al4V in new m-5xSBF, Surf. Coating. Technol. 351 (2018) 1–10.
[39] C. Cao, Principles of Electrochemistry of Corrosion, third ed., Chemical Industry Press, Beijing, 2008.
[40] Z.Q. Zhang, L. Wang, M.Q. Zeng, R.C. Zeng, M.B. Kannan, C.G. Lin, Y.F. Zheng, Biodegradation behavior of micro-arc oxidation coating on magnesium alloy-from a protein perspective, Bioact. Mater. 5 (2) (2020) 398–409.
[41] Q.S. Dong, Z.X. Ba, Y.Q. Jia, Y.J. Chen, X.Y. Lv, X.B. Zhang, Z.Z. Wang, Effect of solution concentration on sealing treatment of Mg-Al hydrotalcite film on AZ91D Mg alloy, J. Magnes. Alloy. 5 (3) (2017) 320–325.
[42] Z.B. Wang, H.X. Hu, C.B. Liu, Y.G. Zheng, The effect of fluoride ions on the corrosion behavior of pure titanium in 0.05 M sulfuric acid, Electrochim. Acta 135 (2014) 526–535.
[43] J. Gonzalez, R.Q. Hou, E.P.S. Nidadavolu, R. Willumeit-Romer, F. Feyerabend, Magnesium degradation under physiological conditions - best practice, Bioact. Mater. 3 (2) (2018) 174–185.
[44] C.Y. Li, L. Gao, X.L. Fan, R.C. Zeng, D.C. Chen, K.Q. Zhi, In vitro degradation and cytocompatibility of a low temperature in-situ grown self-healing Mg-Al LDH coating on MAO-coated magnesium alloy AZ31, Bioact. Mater. 5 (2) (2020) 364–376.
[45] Z.M. Shi, A. Atrens, An innovative specimen configuration for the study of Mg corrosion, Corrosion Sci. 53 (1) (2011) 226–246.
[46] R.C. Zeng, L. Sun, Y.F. Zheng, H.Z. Cui, E.H. Han, Corrosion and characterisation of dual phase Mg-Li-Ca alloy in Hank's solution: the influence of microstructural features, Corrosion Sci. 79 (2014) 69–82.
[47] H.C. Ding, H.H. Pan, X.R. Xu, R.K. Tang, Toward a detailed understanding of magnesium ions on hydroxyapatite crystallization inhibition, Cryst. Growth Des. 14 (2) (2014) 763–769.
[48] X.D. Yang, B.Q. Xie, L.J. Wang, Y.L. Qin, Z.J. Henneman, G.H. Nancollas, Influence of magnesium ions and amino acids on the nucleation and growth of hydroxyapatite, CrystEngComm 13 (4) (2011) 1153–1158.
[49] M.H. Salimi, J.C. Heughebaert, G.H. Nancollas, Crystal-Growth of calcium phosphates in the presence of magnesium-ions, Langmuir 1 (1) (1985) 119–122.
[50] J.D. Termine, A.S. Posner, Infrared analysis of rat bone - age dependency of amorphous and crystalline mineral fractions, Science 153 (3743) (1966) 1523–1525.
[51] M. Nagano, T. Nakamura, T. Kokubo, M. Tanahashi, M. Ogawa, Differences of bone bonding ability and degradation behaviour in vivo between amorphous calcium phosphate and highly crystalline hydroxyapatite coating, Biomaterials 17 (18) (1996) 1771–1777.